Supporting Information

Bio-inspired interfacial chemistry for the fabrication of a robust and functional graphene oxide composite film

Yoo-Bin Kwon,[a] *Seongwon Cho,*[b] *Dal-Hee Min,*[a]* *and Young-Kwan Kim*[b]*

[a]Department of Chemistry, Seoul National University, Seoul 08826, Republic of Korea

[b]Department of Chemistry, Dongguk University, 30 Pildong-ro, Jung-gu, Seoul, 04620, Republic of Korea

* To whom correspondence should be addressed.

Prof. Dal-Hee Min, E-mail: dalheemin@snu.ac.kr

Prof. Young-Kwan Kim, E-mail: kimyk@dongguk.edu

Supporting figures

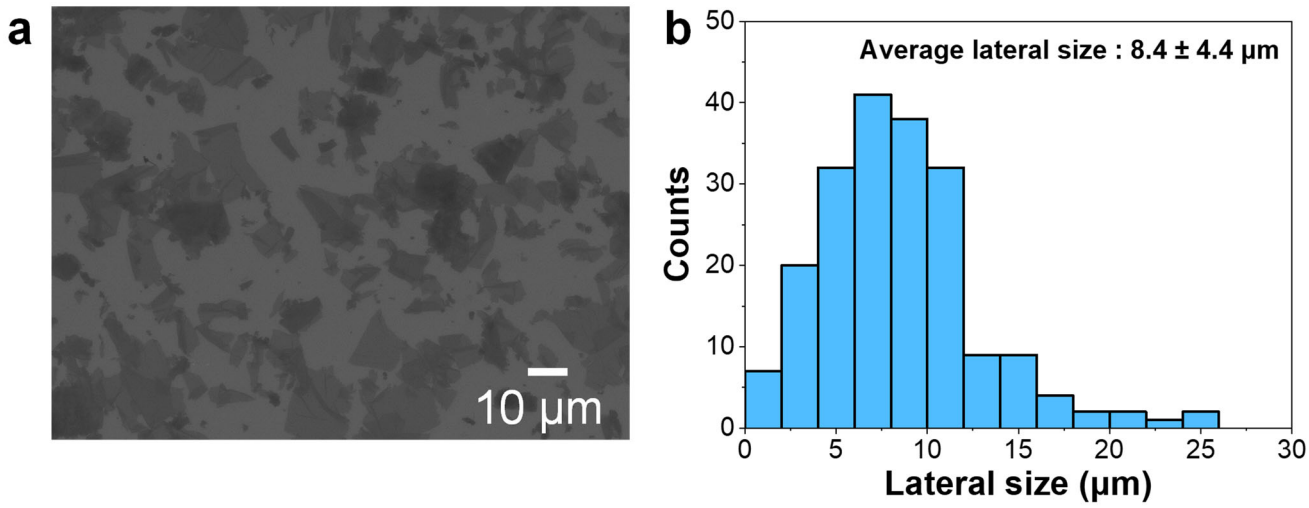

Fig. S1 (a) SEM image and (b) lateral size distribution of GO.

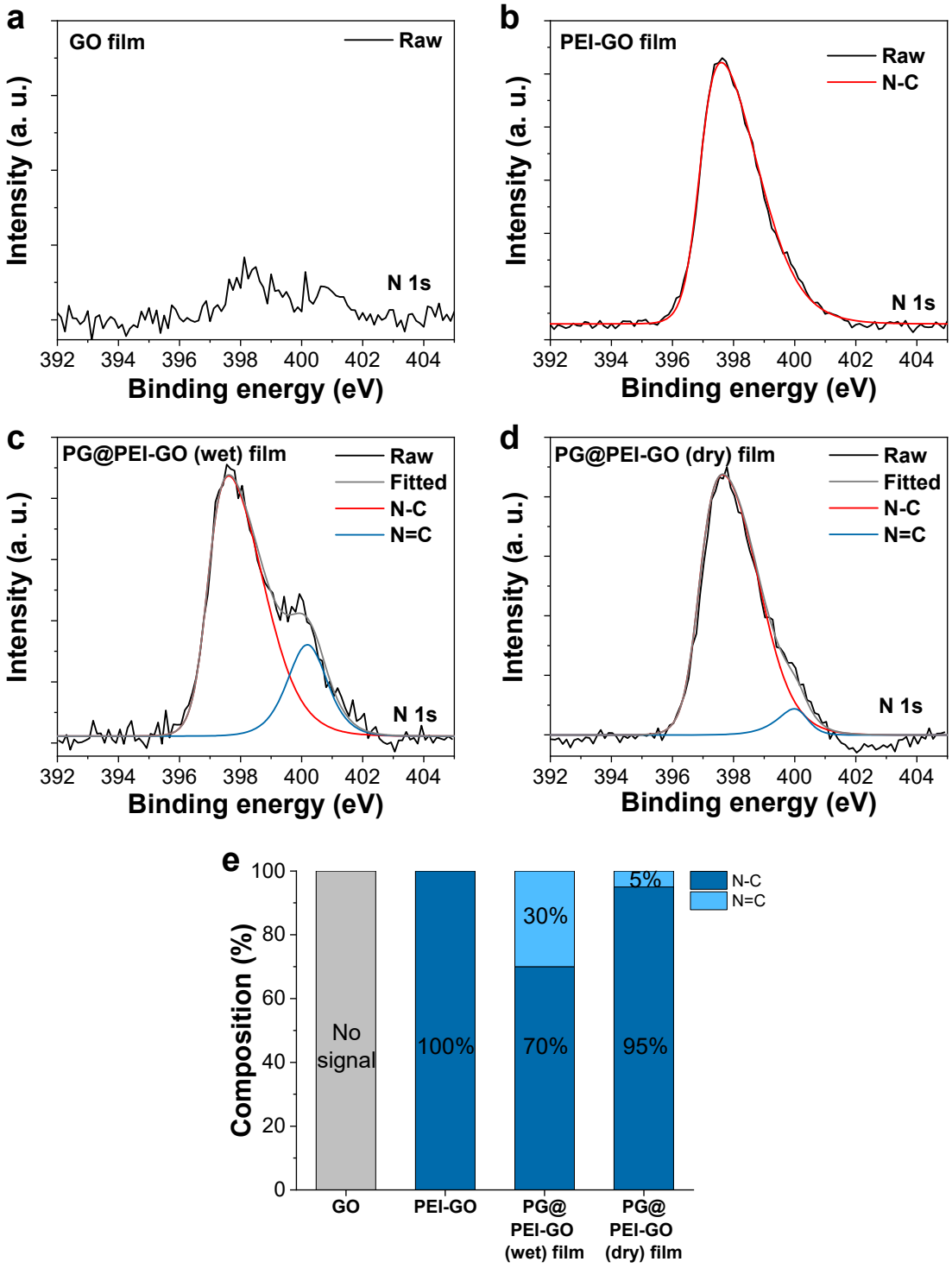

Fig. S2 N 1s XPS spectra of (a) GO, (b) PEI-GO, (c) PG@PEI-GO (wet), and (d) PG@PEI-GO (dry) films and (e) composition of N-C and N=C in those films.

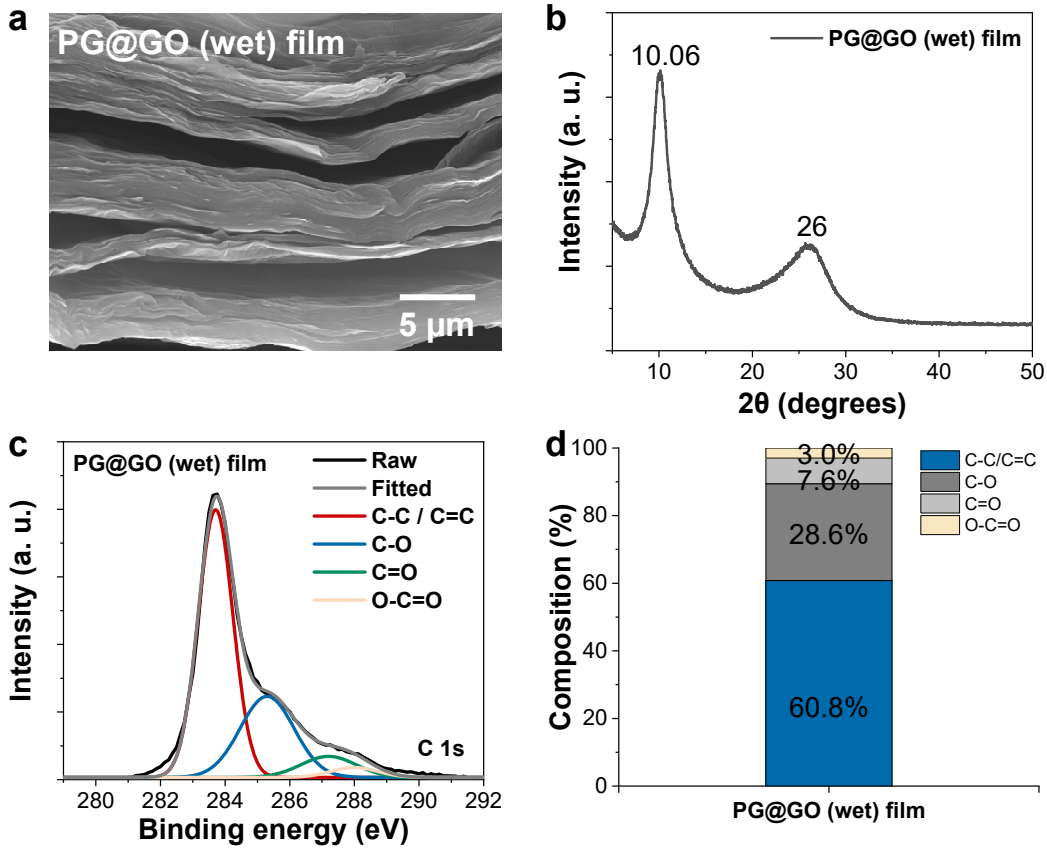

Fig. S3 (a) Cross-sectional SEM images, (b) XRD pattern, (c) C 1s XPS spectra of PG@GO (wet) film, and (d) composition C-C/C=C, C-O, C=O, and O-C=O bonds in PG@GO (wet) film. PG@GO films were fabricated by wet method as a control group. The cross-sectional SEM image of PG@GO (wet) film showed that they were successfully assembled into the nacre-liked films. The XRD and XPS analysis was further performed on PG@GO (wet) films to elucidate their assembled and chemical structures. In their XRD pattern, the (001) diffraction peak of PG@GO (wet) films shifted from 2θ = 10.36° to 10.08° corresponding to d-spacing of 8.53 Å to 8.76 Å. The shift of (001) diffraction peak was due to the intercalated PG in the interlayer of GO films, leading to the enlarged d-spacing between GO sheets. Then, a new band was observed at 2θ = 26° corresponding to d-spacing of 3.42 Å, which originated from the reduced interlayer distance of GO sheets due to the deoxygenation of GO by intrinsic reducing property of PG. In C 1s XPS analysis, PG@GO (wet) films showed typical peaks at 283.7 eV from C-C and C=C bonds (60.8%), 285.8 eV from C-O bonds (28.6%), 287.2 eV from C=O bonds (7.6%), and 288.2 eV from O-C=O bonds (3%). As a result of PG introduction, the composition of oxygen containing bonds decreased, implying the GO was reduced by PG, and it was well-matched with the results of XRD analysis.

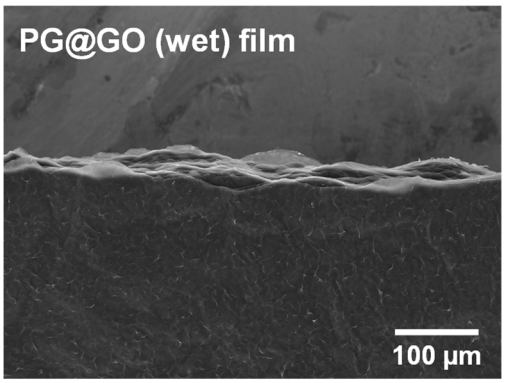

Fig. S4 SEM image of tensile-fractured films of PG@GO (wet) film.

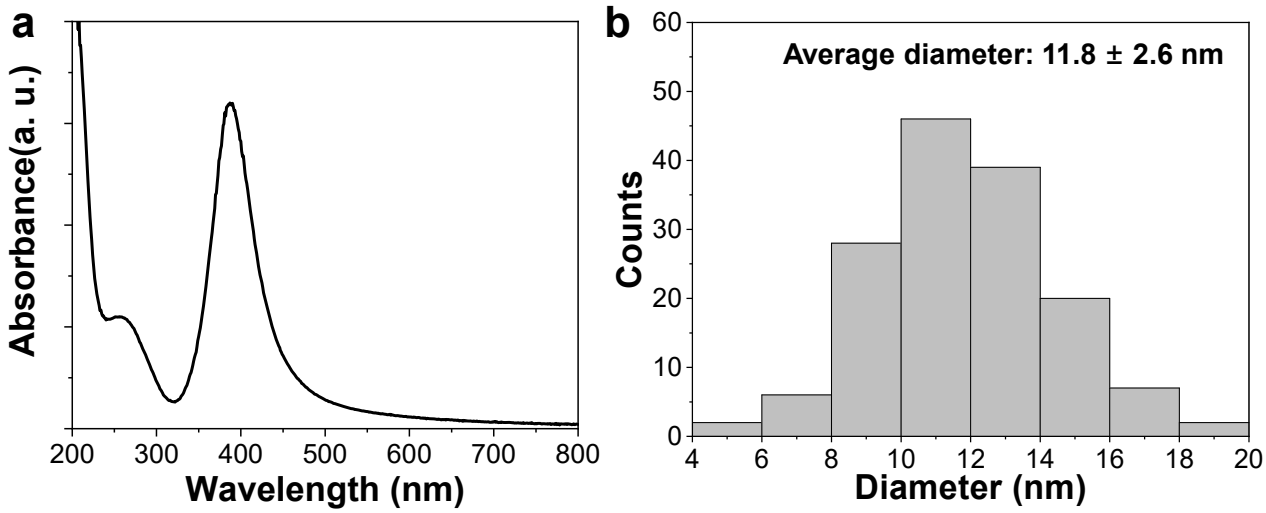

Fig. S5 (a) UV-vis spectrum and (b) diameter histogram of AgNPs. The AgNPs exhibited a typical localized surface plasmon resonance (LSPR) band at around 390 nm and have spherical shape with an average diameter of 11.8 ± 2.6 nm.

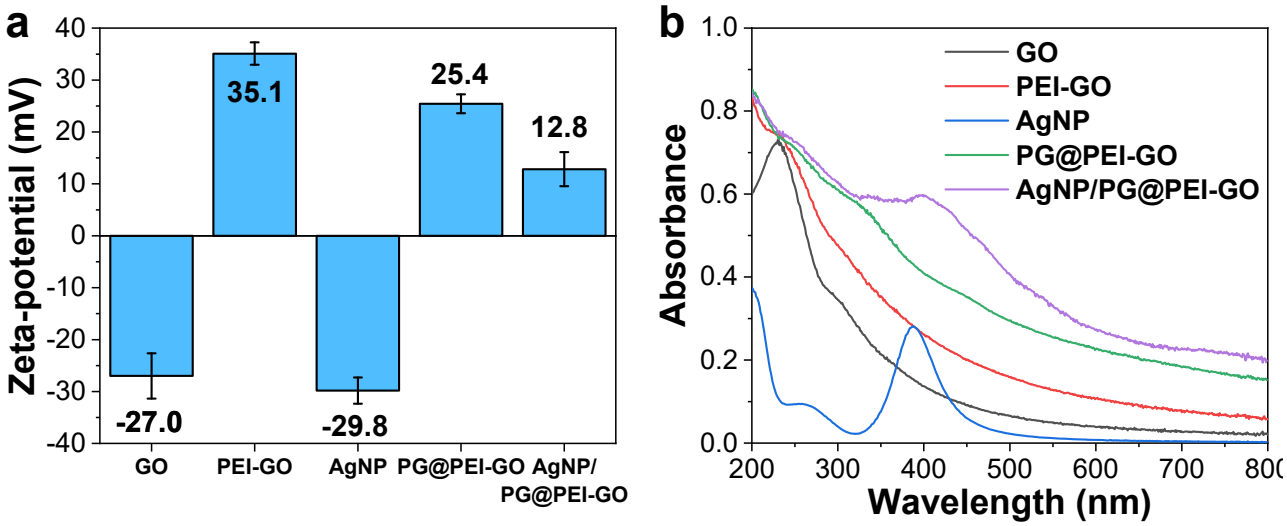

Fig. S6 (a) zeta-potential values and (b) UV-vis spectra of GO, PEI-GO, AgNP, PG@PEI-GO, and AgNP/PG@PEI-GO. The absorbance of PEI-GO in UV region increased after reaction with PG, indicating the increase of aromatic structure through formation of a polyphenol-like structures on its surface through Schiff-base reaction. The synthesized AgNPs has a typical localized surface plasmon resonance (LSPR) band at 390 nm. After incubation of PG@PEI-GO with AgNPs, the resulting AgNP/PG@PEI-GO showed analogous UV-Vis spectrum to PG@PEI-GO except a broad absorption band at around 425 nm which was derived from the slight aggregation and dielectric constant change of AgNPs on the surface of PG@PEI-GO. This result clearly indicated that AgNPs were successfully immobilized on the surface of PG@PEI-GO.

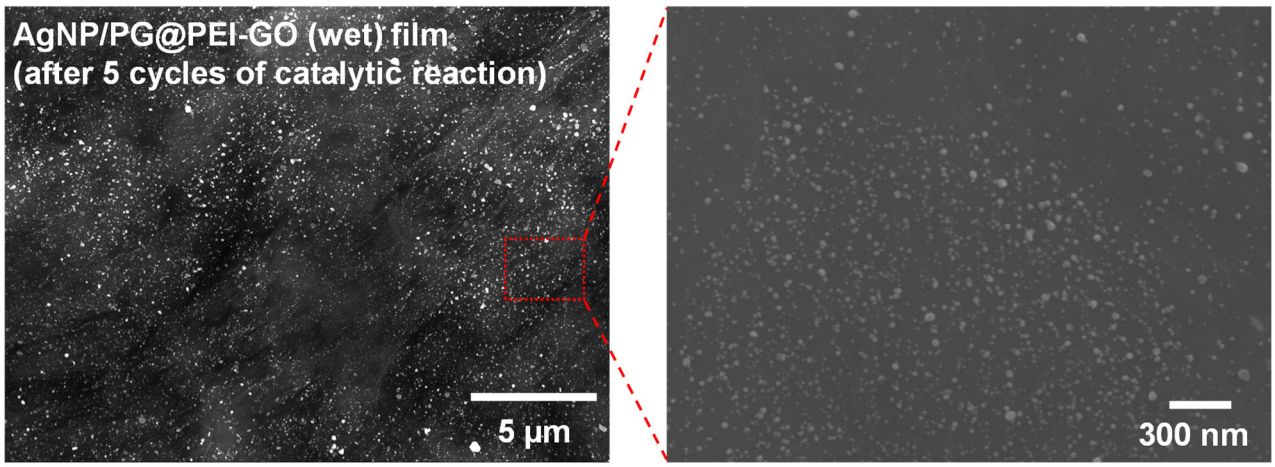

Fig. S7 SEM images of AgNP/PG@PEI-GO (wet) film after 5 cycles of catalytic reaction with different magnifications.

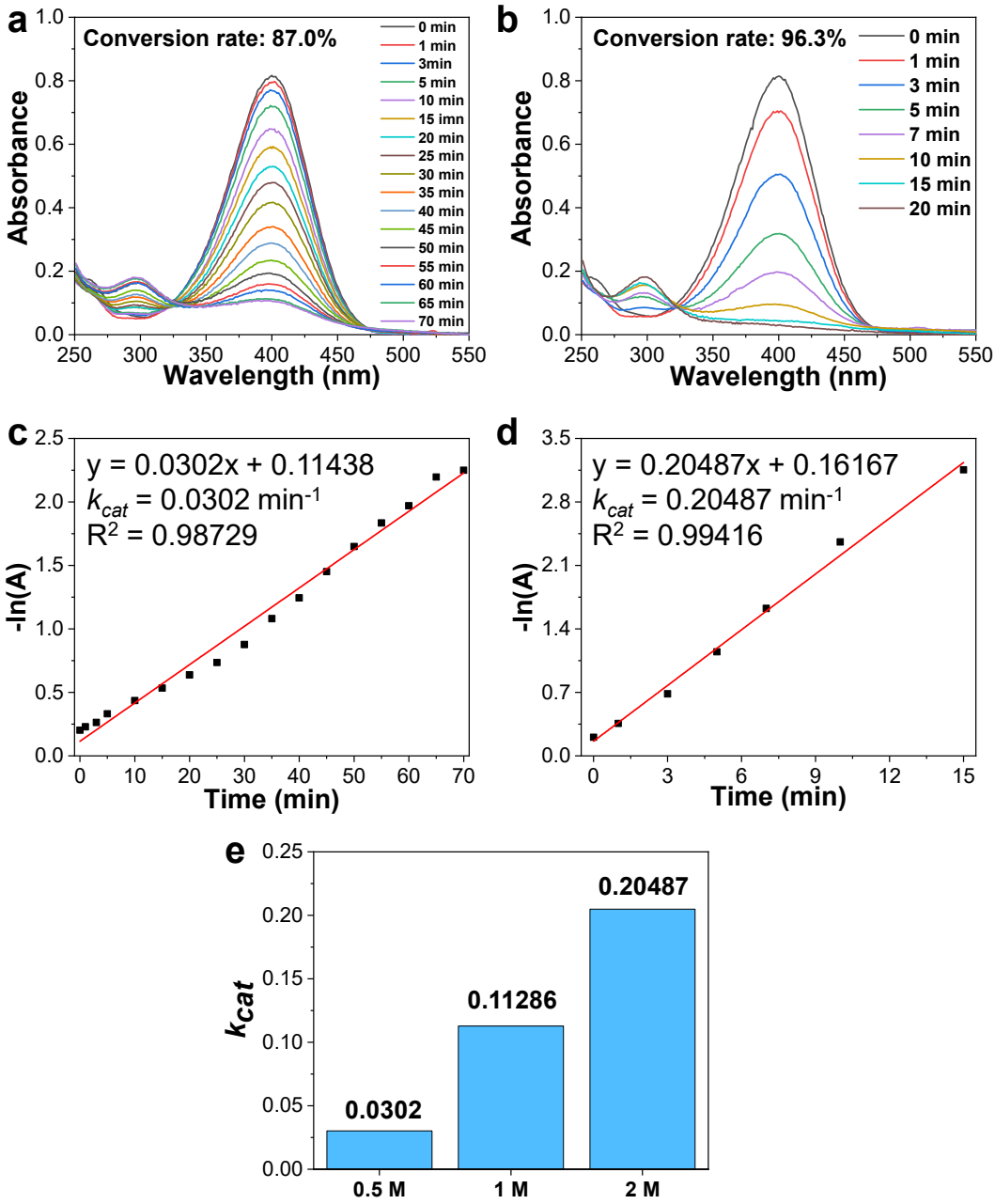

Fig. S8 UV-vis spectra of the catalytic reaction solution using (a) 0.5 and (b) 2 M $NaBH_4$ solutions with AgNP/PG@PEI-GO (wet) film as a function of reaction time. Kinetic analysis of the catalytic reaction using (c) 0.5 and (d) 2 M $NaBH_4$ solutions. (e) Rate constant of catalytic reaction as a function of $NaBH_4$ concentrations.

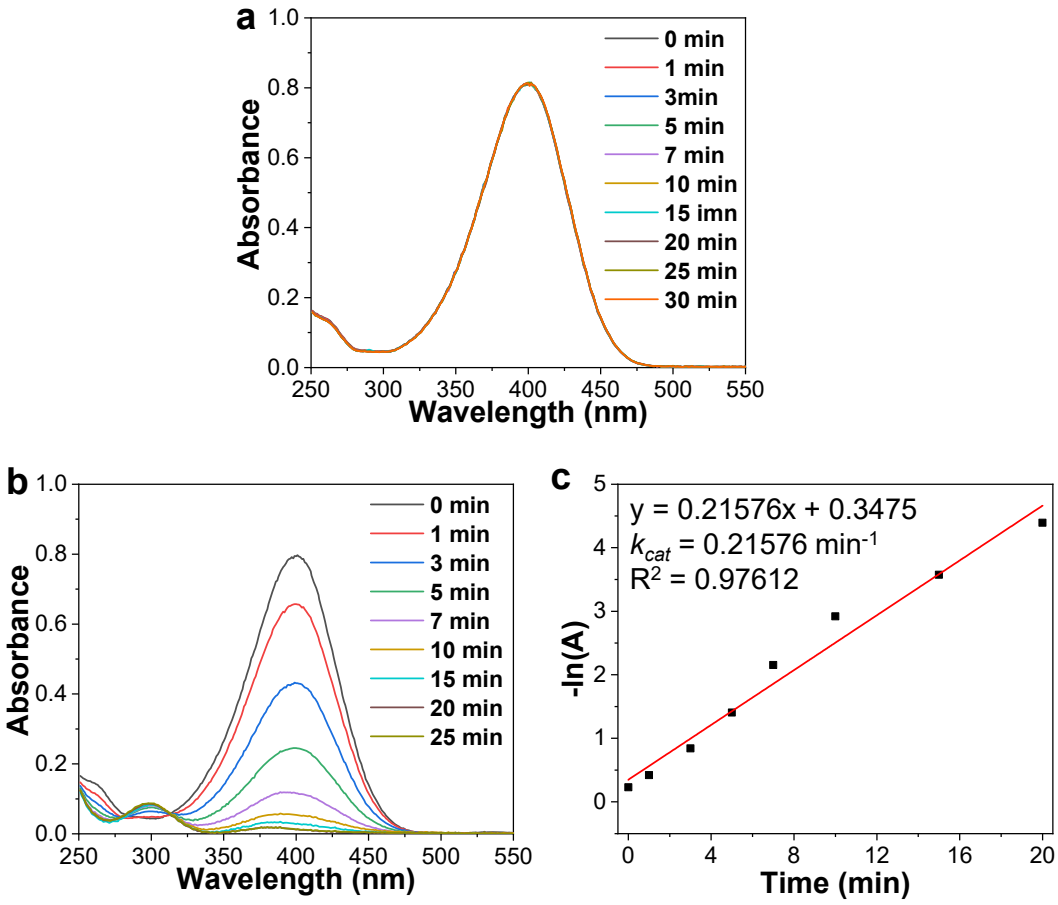

Fig. S9 UV-vis spectra of the catalytic reaction solution with (a) PG@PEI-GO (wet) film and (b) AgNP colloidal solution as a function of reaction time. (c) Kinetic analysis of the catalytic reaction using AgNP colloidal solution.

No.	Catalytic materials	Structures	k_{cat} (min^{-1})	References
1	AuNP/GO/CNT	film	0.0402	1
2	AuNP/activated carbon	membrane	0.0296	2
3	AuNP/CNT	membrane	0.277	3
4	AuNC/CNT	membrane	0.2	4
5	PdNP/PAA/PVA/CNT	film	0.43	5
6	AgNP/nanocellulose	membrane	0.195	6
7	AgNP/PVA/RGO	film	0.048	7
8	PtNP/CNF-PEI	aerogel	0.12	8
9	AuNP/CNT	fiber	0.105	9
10	AgNP/g-C_3N_4/PE	fabric	0.462	10
11	AgNP/GO/P4VP/PAA	hydrogel	0.977	11
12	AgNP/PG@PEI-GO	film	0.11286 (1 M $NaBH_4$) 0.20487 (2 M $NaBH_4$)	This work

Table S1. Comparison of the rate constant with other reported catalysts using noble metal catalysts supported on structural materials.

References

(1) F. Yang, C. Wang, L. Wang, C. Liu, A. Feng, X. Liu, C. Chi, X. Jia, L. Zhang and Y. Li, *RSC Adv.*, 2015, **5**, 37710–37715.

(2) S. Bolisetty and R. Mezzenga, *Nat. Nanotechnol.*, 2016, **11**, 365–371.

(3) Q. Zhang, X. Fan, H. Wang, S. Chen and X. Quan, *RSC Adv.*, 2016, **6**, 41114–41121.

(4) Y. Liu, Y. Zheng, B. Du, R. R. Nasaruddin, T. Chen and J. Xie, *Ind. Eng. Chem. Res.*, 2017, **56**, 2999–3007.

(5) R. Wang, Q. Liu, T. Jiao, J. Li, Y. Rao, J. Su, Z. Bai and Q. Peng, *ACS Omega*, 2019, **4**, 8480–8486.

(6) T. K. Das, S. Remanan, S. Ghosh and N. C. Das, *J. Environ. Chem. Eng.*, 2021, **9**, 104596

(7) K. Sharma, S. Majhi, M. Ali, R. Singh, C. Shekhar Pati Tripathi and D. Guin, *ChemistrySelect*, 2021, **6**, 6071–6076.

(8) H. Yu, S. Oh, Y. Han, S. Lee, H. S. Jeong and H. J. Hong, *Chemosphere*, 2021, **285**, 131448

(9) Y. K. Kim, Y. J. Kim, J. Park, S. W. Han and S. M. Kim, *Carbon*, 2021, **173**, 376–383.

(10) A. Amedlous, M. Majdoub, Z. Anfar and E. Amaterz, *Catalysts*, 2021, **11**, 1533

(11) L. Zhang, L. Sun, T. Su, T. Chen, L. Hu, F. He and H. Xu, *Colloids Surfaces A Physicochem. Eng. Asp.*, 2022, **640**, 128410